Developments in Environmental Science, Volume 8
A. Bytnerowicz, M. Arbaugh, A. Riebau and C. Andersen (Editors)

ISSN: 1474-8177/DOI:10.1016/S1474-8177(08)00006-5

Chapter 6

Airborne Remote Sensing of Wildland Fires

*Philip J. Riggan** *and Robert G. Tissell*

Abstract

In wildland fire management, reliable fire intelligence is needed to direct suppression resources, maintain firefighter safety, predict fire behavior, mitigate fire effects in the environment, and justify and evaluate the effectiveness of fuel management. Fire intelligence needs to be synoptic, quantitative, consistent, and timely. Airborne remote sensing with specialized infrared radiometers is now providing an unprecedented level of information on fire behavior and effects. The temperature, radiant intensity, carbon and sensible heat fluxes, and fuel consumption associated with the flaming front of a wildland fire have been estimated by remotely measuring its radiance at short- and mid-wave infrared wavelengths. Measurements of upwelling long-wave or thermal-infrared radiation provide estimates primarily of ground-surface temperatures, even beneath flaming fronts, that reflect a local time course of energy release and fuel consumption. Characteristics of flames and hot ground can be discriminated from radiances measured at wavelengths near 1.6, 3.9, and 11.9 μm. Fire radiance at 3.9 μm appears to be a good estimator of radiant-flux density, which integrates across wavelengths. There are strong temperature gradients along and within flaming fronts, and although their temperatures are high—commonly exceeding 1000°C along the line of a savanna fire, for instance—flames may not be bright when compared with a blackbody radiator. The combination of that low bulk emissivity and uncertainty as to the composition and radiance of nonfire background within the sensor's instantaneous field of view dictates that fire properties are best estimated from measurements of high spatial resolution in comparison with the scale of a fire front. The USDA Forest Service is now applying a FireMapper™ thermal-imaging radiometer for fire research and support of incident

*Corresponding author: E-mail: priggan@fs.fed.us

command teams over high-priority wildland fires, especially those threatening cities and communities in southern California. Resulting data are providing insight into fire behavior in complex and changing fuels, fire interactions with the atmosphere and a changing climate, and large-scale fire processes.

6.1. Introduction

Large wildland fires burning under high winds in highly flammable fuels and with high values at risk—such as during the October 2007 fire emergency in southern California—demand sophisticated monitoring and communication of fire activity and spread. For tactical firefighting in such situations, reliable fire intelligence and an ability to understand and predict fire behavior are needed to effectively deploy resources—engines, personnel, and aircraft; to keep firefighters safe; and to tailor the allocation of resources to the fire, reducing the need to commit more resources than necessary and reducing costs of suppression. After the emergency, data on fire severity are needed to mitigate fire effects in the environment. On a strategic level, an ability to accurately predict fire behavior is requisite to design, justify, and evaluate approaches for fire management, including landscape-scale fuel treatments.

Modern remote sensing can supply the intelligence needed for fire management and the data required for understanding and modeling fire behavior and effects in the environment. Frequent, high-resolution remote sensing at infrared wavelengths can track fire-line rate of spread and acceleration, the location and rates of spotting ahead of a fire front, and structure ignition in residential communities. Together with global positioning system (GPS)-based asset tracking, remote sensing could improve firefighter safety by showing incident commanders the spatial relation of firefighters and equipment to the fire, and especially to regions of high fire intensity or activity. High-resolution imaging also has the potential to accurately quantify large-fire energy release or intensity, residence time, fuel consumption rate, carbon emissions, and soil heating (Riggan & Hoffman, 2003; Riggan et al., 2004). The challenge is to deduce meaningful and useful fire properties based on measurements of upwelling infrared radiation, which will penetrate smoke, with some attenuation depending on wavelength, but not condensed-water clouds.

At present in the United States, national airborne infrared mapping operations collect fire imagery at night with fire-perimeter maps made available for early morning briefings of the incident-management team.

Fire locations during active burning periods in daylight hours are generally known from flights by helicopter along a fire's perimeter and ad hoc ground-based observations and verbal descriptions obtained from low-level aircraft flights, both of which are hindered by obscuring smoke and terrain and a limited field of view. Perimeter maps have the disadvantage of showing where the fire has been, but not necessarily where it is active, intense, or spreading, especially if not provided in real time.

To realize the promise of infrared fire imaging, one must make the proper measurements, and infrared imagers and imaging spectrometers traditionally used for earth remote sensing typically are saturated by—and incapable of measuring—the very bright infrared light that radiates from large wildland fires (Fig. 6.1). Thus, they provide a limited or even

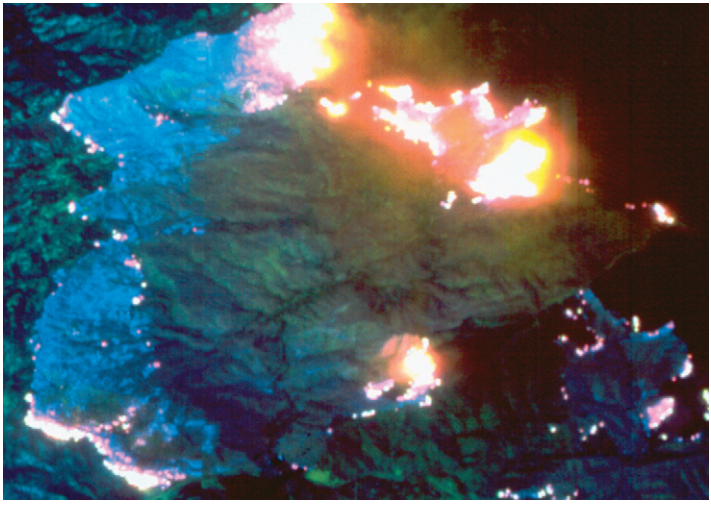

Figure 6.1. Color-composite infrared image of the 1985 Wheeler Fire, Los Padres National Forest, as viewed by the NASA Thematic Mapper Simulator aboard a high-altitude ER-2 aircraft (image courtesy of J.A. Brass, NASA Ames Research Center). In this depiction, using infrared channels nominally at 1.65-, 2.0-, and 8–12.5-μm wavelength, the fire line is comprised of an 8-km-long segment on the north, which generated a large plume reaching to over 19,000 ft altitude (top); burning in a riparian area (lower left); an inactive line (on the west); and a recent backfire north of Ojai, CA (lower right). Saturation of the preamplifiers in the Daedalus ADD 1268 line scanner at relatively low radiances caused a distorted view of fire activity, such as on the north where fire fronts appear to be over 1 km wide yet are likely much less than one-tenth that width. Even though the imager can map the fire through heavy smoke and show its location in terrain, it grossly distorts the magnitude of the fire activity and allows no estimates of fire intensity or impact (Riggan & Hoffman, 2003).

distorted view of fire activity. Furthermore, infrared line scanners, as currently used in fire operations in the United States, are expensive to procure and maintain, and require strong engineering support. They are typically deployed nationally, and thus may be infrequently available or unavailable to a given fire incident. Forward-looking infrared imagers designed for surveillance at common earth temperatures have also been used locally to map fire lines, but these also typically saturate at relatively low brightness values and may be even incapable of discriminating fire from warm ground or ash.

The USDA Forest Service's Pacific Southwest Research Station (PSW) and its partners, NASA Ames Research Center and Space Instruments, Inc., have developed and applied remote-sensing systems for airborne, high-resolution fire mapping and measurement. These have included an extended-dynamic-range imaging spectrometer, a line scanner operating in three regions of the infrared spectrum with channels centered at wavelengths of 1.63, 3.9, and 11.9 μm (Riggan et al., 1993, 2004), and the FireMapper™ thermal-imaging radiometer, which uses a modern microbolometer focal-plane array to image and measure thermal-infrared radiation at wavelengths from 8 to 12.5 μm (Riggan & Hoffman, 2003; Riggan et al., 2003).

In this chapter we will review the basis for quantifying large-fire properties by remote sensing and provide examples from airborne measurement with these instruments of fires in Mediterranean-type ecosystems in southern California and savanna and tropical forests of Brazil.

6.2. Estimating fire properties by remote sensing

6.2.1. Fire front temperatures and the emissivity-fractional area

Wildland fires present a complex remote-sensing target comprised of flaming fronts, ash, residual flaming combustion, smoldering of larger biomass elements, and unburned vegetation (Riggan et al., 2004), arrayed in a scene of complex spatial temperature gradients. Observations at high-resolution provide an opportunity of resolving these components and gradients. Low-resolution observations, as with some satellite-based sensors, such as the Moderate Resolution Imaging Spectrometer (MODIS) or Advanced Very High-Resolution Radiometer (AVHRR), will necessarily encompass radiation from a variety of these elements. In either case, atmospheric windows in the infrared, where radiation is not strongly absorbed by water vapor, dictate that observations may

generally be made at wavelengths near 1.6, 2, and 4 μm in the short- and mid-wave infrared region and from 8 to 14 μm in the long-wave or thermal infrared.

To estimate fire properties by remote sensing it has been assumed that the radiant emissions from flames are primarily from entrained, glowing soot particles and that hot soot and ash approximate classic and highly efficient (or emissive) gray-body radiators whose properties are described by the Planck function (as given, e.g., by Liou (1980)). With these assumptions, the temperature, T, of a hot target within a flaming zone can be estimated by an iterative solution (Eq. 6.1) of two instances of the Planck function (referred to herein as the two-channel method), using the radiance, B, measured at each of two infrared wavelengths, λ_1 and λ_2 (Matson & Dozier, 1981; Riggan et al., 2004)

$$T = \frac{hc}{k\lambda_1 \ln\left[\left(\frac{B_2}{B_1}\right)\left(\frac{\lambda_2^5}{\lambda_1^5}\right)\left(\exp\left(\frac{hc}{k\lambda_2 T}\right) - 1\right) + 1\right]} \tag{6.1}$$

where h is the Planck constant, 6.63×10^{-34} (J.s); c is the speed of light, 3.00×10^8 ($m\,s^{-1}$); k is the Boltzmann constant, 1.38×10^{-23} ($J\,K^{-1}$); T is specified in Kelvin; λ is in meters, B_λ has units of $J\,m^{-2}\,s^{-1}\,sr^{-1}\,\mu m^{-1}$, and radiances are corrected for atmospheric transmittance and path radiance. Note that an iterative solution is required since T is found on each side of Eq. (6.1); the solution can begin with a temperature estimate (Eq. 6.2) derived from a simplification of Eq. (6.1)

$$T = \frac{hc\left(1/\lambda_2 - 1/\lambda_1\right)}{k \ln\left[\left(B_1\lambda_1^5/B_2\lambda_2^5\right)\right]} \tag{6.2}$$

A solution that converges to a temperature within 0.1 K is obtained within six iterations when wavelengths near 1.6 and 3.9 μm are used. These wavelengths are optimal for estimating flame temperatures since they fall on either side of the expected maximum in flame radiance.

The temperature and radiance at one wavelength can be used to estimate the product of the unitless *emissivity*, ε, and the *fractional area*, A_f, of the hot target within the instantaneous field of view of the sensor (Eq. 6.3)

$$\varepsilon A_f = \frac{B_i\lambda_i^5\left[\exp(hc/k\lambda_i T) - 1\right]}{2 \times 10^{-6} hc^2} \tag{6.3}$$

The latter parameter will be meaningful where the observations are of sufficient resolution that the radiance of the hot target is predominant in relation to unburned or cooled ground.

The fire's wavelength-integrated radiant-flux density, F_d ($\mathrm{J\,m^{-2}\,s^{-1}}$), a measure of radiant fire intensity, can be estimated from the combined emissivity-fractional area and flame temperature as

$$F_d = \varepsilon A_f \sigma T^4 \tag{6.4}$$

where σ is the Stefan–Boltzmann constant, $5.67 \times 10^{-8}\,\mathrm{J\,m^{-2}\,s^{-1}\,K^{-4}}$.

Riggan et al. (2004) mapped the apparent flame temperatures and radiant-flux density of large fires in Brazil by using this two-channel method and high-spatial-resolution remote-sensing observations with an extended-dynamic-range spectrometer at short- and mid-wave infrared wavelengths of 1.63 and 3.9 μm. Flame radiances at these wavelengths were sufficiently high so that contributions to the signal from reflected solar radiation could be ignored.

Among the most extensive measurements made were those of the Tapera prescribed fire on September 21, 1992, at the Reserva Ecológica of the Instituto Brasileiro de Geographia e Estatística (the Ecological Reserve of the Brazilian Institute of Geography and Statistics) in the Brazilian Federal District (Riggan et al., 2004). This fire burned within a watershed of low relief with vegetation comprised of three phases of the Cerrado ecosystem—campo cerrado, campo sujo, and campo limpo—which represent a gradient of tropical-savanna plant communities in which evergreen shrubs comprise a declining proportion of the plant cover in a grassland matrix. Biomass structure in these communities has been described by Ottmar et al. (2001).

Remote-sensing observations showed that 90% of the Tapera fire's radiant-flux density was associated with temperatures between 731°C and 1042°C with the 50th percentile for those radiant emissions associated with a temperature of 879°C. There were strong temperature gradients across and along fire lines, with temperatures at actively spreading fire fronts occasionally exceeding 1300°C (Fig. 6.2). The mean of *peak* temperatures observed along a fire front in one instance of the Tapera fire was 1050°C (SD = 108°C) with an associated emissivity-fractional area of 0.045 (SD = 0.021). Over a 40-minute course of burning, which encompassed most of the active spread by the fire, the mean radiometric fire temperature varied only from 824 to 852°C; thus a whole-fire temperature estimate, as might be obtained from low-spatial-resolution observations by satellite, would not provide much information regarding changes in fire activity. Temperature estimates from remote sensing of the fire compared favorably with temperatures measured with thermocouples in flames near the ground (Riggan et al., 2004).

Fire temperatures and radiant-flux densities associated with a fire burning in partially harvested and slashed tropical forest near Marabá,

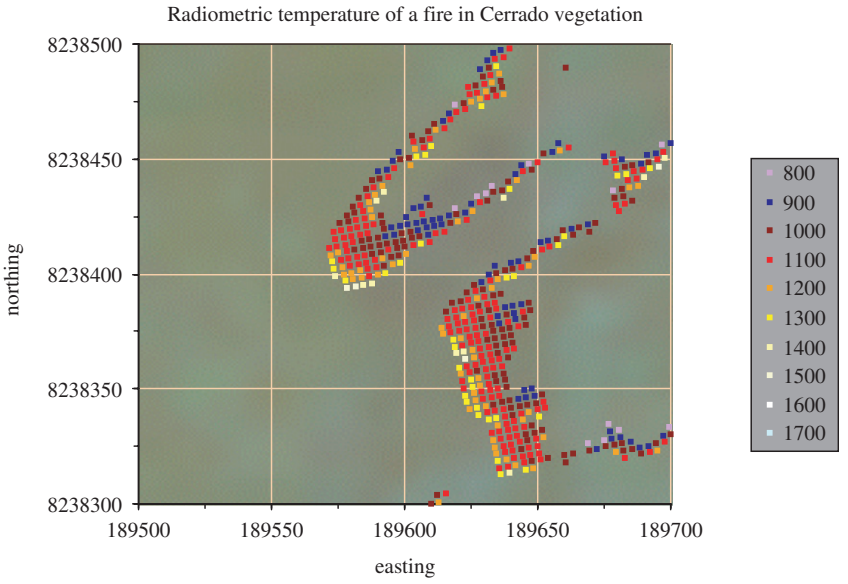

Figure 6.2. Radiometric temperatures (Kelvin) of a portion of the Tapera fire spreading in Cerrado vegetation, a form of tropical savanna, in central Brazil. Temperatures are estimated from radiances observed at 1.63- and 3.9-μm wavelengths by an extended-dynamic-range imaging spectrometer (Riggan et al., 2004). Here, fire is spreading with the wind from northeast to southwest. Temperatures are generally elevated along the leading edge of the two fire lobes and reduced behind the front and along the fire's flanks. Fire location is shown in Universal Transverse Mercator (UTM) coordinates.

Brazil, reflected a high-intensity front with extensive reaches of residual combustion of woody debris (Fig. 6.3a) (Riggan et al., 2004). The residual combustion was especially important to the overall radiant-flux density of the fire: only 17% of that measure for the slash fire was associated with temperatures greater than 800°C; 17% of the flux density from the Tapera fire was associated with temperatures *below* that value (Fig. 6.4). *Peak* temperatures, sampled at a 3.5-m interval along a 250-m flaming front spreading with low winds, had a mean value of 1021°C (SD = 284°C, $n = 250$), which was remarkably similar to that observed in the Tapera fire, which primarily burned grass.

Even though flames of Cerrado fires appeared quite hot, they were not especially bright when compared with a solid blackbody radiator. Observations from across the flaming front of the Tapera fire, for instance, showed that flames were optically thin: the mean value of the combined emissivity-fractional area was 0.091, so the radiant-flux density was on average less than one-tenth as great as that expected from a

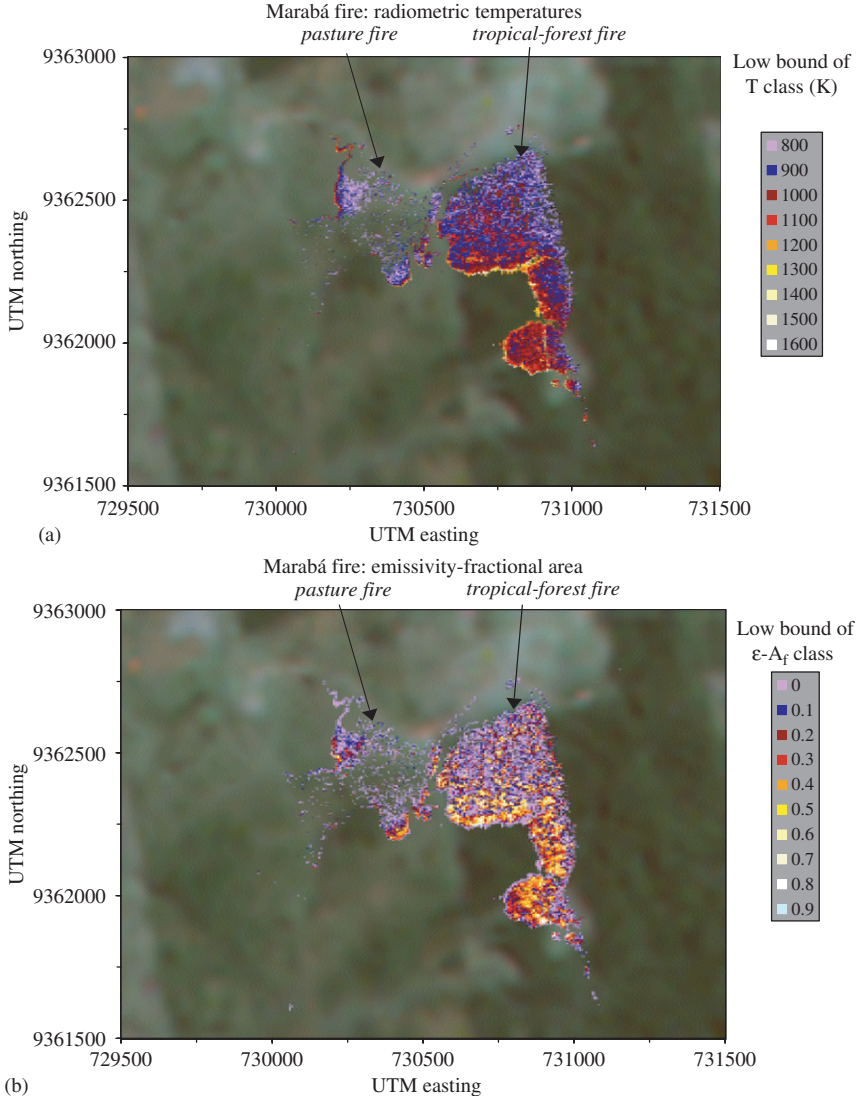

Figure 6.3. (a) Radiometric temperatures of a fire in partially slashed tropical forest and pasture in Brazil as estimated from radiances measured at 1.63- and 3.9-μm wavelengths with an extended-dynamic-range imaging spectrometer. The forest burning, which apparently consumed downed woody debris, was notable for its high-temperature front and extensive reach of cooler residual combustion. Temperatures along the fire line there were greatest where the fire spread with the northeast wind than where it generally spread to the north, unaided by the ambient wind. Tropical vegetation is shown here as imaged by the Landsat Thematic Mapper. (b) Values of the product of emissivity and fractional area for a fire as described in Fig. 6.3a. The forest burning was notable for relatively high values of the product behind the actively spreading, high-temperature, fire front. Pasture burning, west of an easting of approximately 730,600, showed moderate levels of the product at and near the fire front and very low values in residual burning in the interior of the fire area.

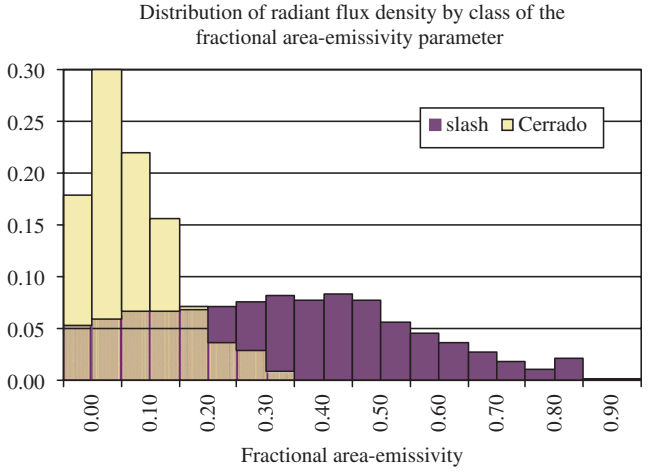

Figure 6.4. Distribution of radiant-flux density by class of the combined emissivity-fractional area for fires burning in slashed tropical forest (shown in purple) and Cerrado or tropical savanna vegetation (in yellow) in central Brazil (Riggan et al., 2004). A relatively large proportion of the emitted energy from burning in slash, which included a high-intensity fire front, was associated with large values of the emissivity-fractional area. Stippled areas in the graphic show overlap between the two histograms.

blackbody at comparable temperatures. Such a low value is suggestive that hot ash beneath a flaming front, which is expected to have an emissivity near 1.0 and is typically cooler than the peak flaming-front temperatures estimated from 1.63- and 3.9-μm radiances, may provide a substantial portion of the upwelling radiation from that front depending on the wavelength of the observation. The emissivity-fractional area observed in the Marabá slash fire obtained high values, approaching one, across a wide reach of ground behind the fire front (Fig. 6.3b).

Peak blackbody temperatures (median = 460°C, SD = 36°C) along flaming fronts in a September 19, 2000, Cerrado fire at the Reserva Ecológica, as estimated from radiances measured with the FireMapper at a *long-wave* infrared wavelength of 11.9 μm, were substantially less than those obtained from wavelengths of 1.63 and 3.9 μm at the nearby Tapera fire, which had burned in similar fuel. The long-wave radiometric temperatures were more consistent with temperatures obtained at the soil surface beneath flaming combustion in Cerrado vegetation (Miranda et al., 1996).

From these combined observations it appears that flames obtain maximum radiance in the short-wave infrared—temperatures observed in Cerrado fires correspond to a radiance peak at a wavelength of

approximately 2.2 μm, and radiation from a high-emissivity, hot-ash surface, whose temperatures correspond with a peak radiance near 4 μm, dominates that from optically thin flames at long infrared wavelengths.

To demonstrate these points we modeled radiances for a Cerrado fire as follows: radiance of flames was assumed to be that of a gray-body radiator with a temperature of 1095°C and an emissivity-fractional area of 0.046, corresponding to an instance of peak fire-line temperatures estimated using measured radiances at 1.63- and 3.9-μm wavelength; the combined emissivity-fractional area of flames and subtending hot ground or ash was assumed to be 1.0; and an assumed temperature of the ash surface beneath the flames was adjusted to obtain the average peak radiometric blackbody temperature along fire lines as estimated under similar circumstances using FireMapper observations at 11.9-μm radiance in the long-wave infrared. An estimated temperature of the ground-surface beneath flames of 426°C results.

The model predicts for observations near the leading edge of a fire front in Cerrado that hot ground and ash contribute approximately 4% of the radiance at 1.63 μm; three-fifths of the radiance at 3.9 μm, and nearly nine-tenths of the radiance at 11.9 μm (Fig. 6.5). Since the 3.9-μm radiance is strongly influenced by both flames and the hot-ash surface beneath, fire temperature estimates obtained from the two-channel method of Eq. (6.1) and wavelengths of 1.63 and 3.9 μm must be influenced by both of these components as well; bulk temperature estimated by that method, 832°C, was intermediate to that of the two included model components. Radiant-flux density, $1.83 \times 10^4\,\mathrm{J\,m^{-2}\,s^{-1}}$, obtained from the bulk temperature, emissivity-fractional area, and an integration of radiance from 1 to 14 μm in this instance, was approximately nine-tenths of that obtained by integration of radiance from the two modeled components, flame, and hot ash. Thus, the two-channel method provided a modest underestimate of the radiant-flux density from the modeled system.

Because the 3.9-μm radiance of a wildland fire has substantial components from both flames and hot ash, we investigated the utility of that radiance alone in predicting the radiant-flux density of the bulk system. Whereas the 1.63-μm radiance provided only a poor predictor, the 3.9-μm radiance ($B_{3.9}$) showed a high and similar correlation with radiant-flux density (F_d) for both the Tapera and Marabá fires (Fig. 6.6). For one remote-sensing observation of the Tapera fire, linear regression with a no-intercept model gave the function $F_d = 17.87(B_{3.9})$, with $r^2 = 0.994$, $n = 712$, and the 95% confidence limit for the slope = {17.81, 17.93}, where n is the number of fire-associated pixels within the image. For the Marabá Fire, linear regression gave the function $F_d = 16.99(B_{3.9})$,

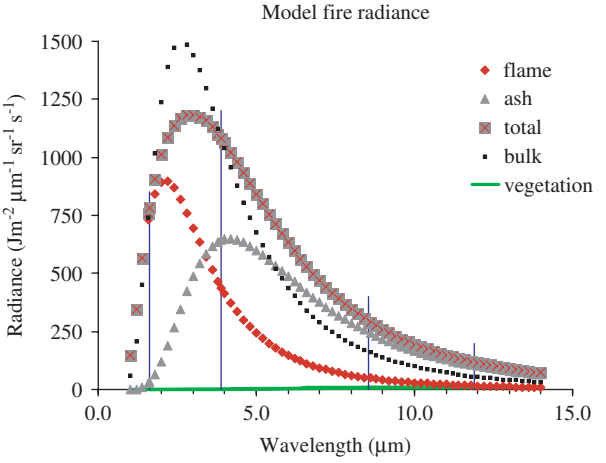

Figure 6.5. Modeled radiances ($J\,m^{-2}\,\mu m^{-1}\,sr^{-1}s^{-1}$) of a fire in Cerrado or tropical savanna. Contributions from flames and hot ash are shown along with a "bulk" temperature computed from a two-channel estimator and measurements at wavelengths of 1.63 and 3.9 µm. The wavelength-integrated radiant-flux density ($J\,m^{-2}s^{-1}$) for the bulk-temperature estimate is 0.89 of that obtained from the total of flame and ash radiances. The very low emitted radiance of vegetation is shown by comparison. Vertical blue bars indicate the wavelengths discussed in the text: 1.63 and 3.9 µm as measured with the NASA/Forest Service extended-dynamic-range imaging spectrometer and 8.6 and 11.9 µm as measured with the Forest Service FireMapper.

with $r^2 = 0.998$, $n = 33{,}333$, and the 95% confidence limit for the slope = {16.986, 16.998}. The small difference between the fires may be due to uncorrected differences in atmospheric transmittance involving the two channels.

6.2.1.1. A three-wavelength method

Our model of the radiances from the Tapera fire points to an improvement in the two-channel method of Eq. (6.1) in which component temperatures of flames and hot ash, emissivity-fractional area for flames, and their contributions to the upwelling radiation are estimated based on radiances measured at three wavelengths and a model where the emissivity-fractional areas of the two components sum to one (Riggan et al., 2000). The three-wavelength algorithm proceeds as follows:

1. Iteratively calculate approximate flame temperature and emissivity-fractional area using the two-channel method and observed radiances near 1.6 and 3.9 µm.

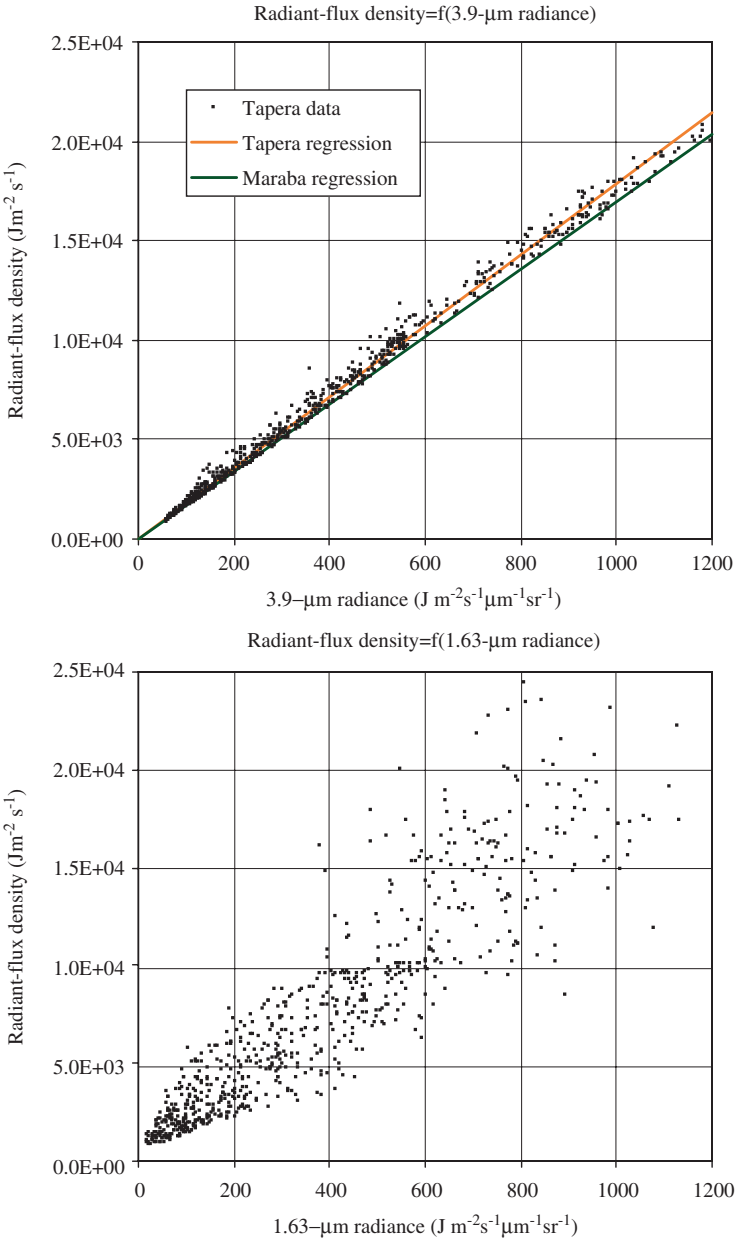

Figure 6.6. Radiant-flux density ($J\,m^{-2}\,s^{-1}$) as a function of single-channel radiances for the Tapera fire in Cerrado vegetation. The 3.9-μm radiance alone provides a good predictor of the flux density as determined by a two-channel solution for fire temperature (top). The 1.63-μm radiance (bottom) does not. The predictor based on the 3.9-μm radiance varies little with the fire situation as shown by the similarity of the two regression equations for the Cerrado and tropical forest fires (top).

2. Calculate the hot-ash or background contribution to the 11.9-μm radiance as the difference between the observed radiance and the flame radiance at that wavelength as estimated in step 1.
3. Estimate the background blackbody temperature and subtract the background contribution to radiances at 1.6 and 3.9 μm from the observed values at those wavelengths.
4. Iterate steps 1– 4 using successive estimates of flame and background radiance until stable estimates of flame temperature and emissivity-fractional area are achieved.

From the modeled two-component system above, the three-wavelength method achieves stable temperature estimates of flame and hot-ash to within 1°C within 10 iterations.

We applied the three-wavelength algorithm to a selection of data from across a fire front in Cerrado in Central Brazil (Riggan et al., 2000). In this case the measurement at 11.9 μm had a relatively low signal-to-noise ratio, so we estimated likely values for individual high-resolution point measurements based on a regression of radiance at 11.9 μm to that at 3.9 μm. The result was that estimated flame temperatures rose by an average of approximately 60°C over that estimated by two channels alone, and the mean background temperature from across the fire was estimated to be 170°C.

We conclude that high-resolution fire-radiance measurements at short- and mid-wave-infrared wavelengths describe the bulk properties of a combination of flame and hot ash, with the greatest contribution to the 1.6-μm radiance arising from flames and substantial contributions to the 3.9-μm radiance from both sources, and that partitioning the 3.9-μm radiance would be useful to account for hot background in the fire signal (Riggan et al., 2000). Measurements in the long-wave infrared, as with the FireMapper, primarily reflect the temperature of hot ash and ground beneath a flaming front.

These estimates provide useful and readily interpretable measures of fire activity that may be applied in fire management (Riggan et al., 2004; Riggan et al., 2003). Radiant-flux density from flames provides the intensity of the fire front and a measure of fuel consumption at the instant of observation, as described below. Integration with time of the radiant-flux density from the hot ground surface is expected to provide a correlative measure of fuel consumption during fire front passage.

6.2.2. Estimating fuel consumption and carbon flux to the atmosphere

Flame radiance and fire areal growth rate measured by remote sensing have provided a provisional but promising estimator for fuel consumption

rate and the rates of carbon and sensible heat flux to the atmosphere (Riggan et al., 2004).

Sensible-heat and carbon fluxes from three large fires in central Brazil were estimated from *in situ* aircraft-based measurements of smoke-plume cross-sectional area and the vertical components of wind velocity, air temperature, and CO_2 mixing ratio within those plumes. Carbon and energy flux per unit area burned were estimated for one fire in Cerrado from the ratio of these whole-fire rates and the associated areal progression of the fire over time ($m^2\,s^{-1}$). The plume-based fuel consumption estimate so derived, $1.1\,kg\,m^{-2}$, compared well with nearby ground-based estimates of biomass loss during burning in somewhat lighter fuels ($0.8–1.0\,kg\,m^{-2}$) (Miranda et al., 1996).

Whole-plume carbon and sensible heat fluxes were then related to *remotely sensed* flame properties by a simple model. The model set the sensible heat flux (Q_s) equal to the product of the density (ρ_{air}) and specific heat (C_p) of moist air, the eddy diffusivity of heat (K_H)—which was assumed proportional to flame temperature (T_f)—and the near-ground potential temperature gradient ($\partial\theta/\partial z$), which was taken as proportional to the difference between flame temperature and that of the overlying ambient air (T_{amb}). Thus,

$$Q_s = \rho_{air} C_p k_T T_f (T_f - T_{amb}) \tag{6.5}$$

With Q_s given in $J\,m^{-2}\,s^{-1}$, ρ_{air} in $g\,m^{-3}$, C_p in $J\,g^{-1}\,K^{-1}$, and T in K, application of the model to remote sensing observations of high-temperature, flaming combustion ($T_f > 1100\,K$) of the Tapera fire in Cerrado vegetation yielded a value of the proportionality constant $k_T = 0.0026$. When applied to observations of a free-burning fire in Cerrado vegetation at the Serra do Maranhão in the Brazilian Federal District and of the tropical-forest slash fire measured at Marabá, this remote-sensing-based model produced estimates of sensible heat flux that were consistent with *in situ* plume measurements from the two fires (Table 6.1). Furthermore, whole-plume carbon flux was strongly correlated with the flux of sensible heat (Riggan et al., 2004). Thus, the rate of fuel consumption by flaming fronts of entire large fires could be estimated from fire radiance at short- and mid-wave infrared wavelengths.

6.2.3. Satellite-based measurements of fire properties

Observations from sensors aboard the National Oceanic and Atmospheric Administration (NOAA) polar orbiting and geostationary environmental satellites and more recently from the NASA MODIS show that radiant

Table 6.1. Estimates of sensible-heat flux as derived from remotely sensed fire properties and from cross-plume airborne measurements for three wildland fires in Brazil (modified from Riggan et al., 2004)

	Cerrado		Tropical forest
	Tapera fire	Serra do Maranhão fire	Marabá slash fire
From remote sensing			
Radiant flux density ($J\,s^{-1}$) for $T > 1100\,K$	4.1×10^7	6.4×10^7	2.8×10^8
Modeled from remote sensing			
Sensible H flux ($J\,s^{-1}$) from fire radiance	8.7×10^8	*1.4×10^9*	**6.4×10^9**
From plume measurements			
Sensible H flux ($J\,s^{-1}$)	8.7×10^8	*1.4×10^9*	**6.7×10^9**

Note: Radiant-flux density is shown for comparison. A proportionality constant, $k_T = 0.0026$, from Eq. (6.5) was determined by setting the remote-sensing-based estimate for the Tapera fire equal to that from airborne measurements; the resultant model was applied to high-temperature remote-sensing data, with $T > 1100\,K$ (827°C), from the Serra do Maranhão and Marabá fires (see values in italic and bold.)

emissions of fires may be readily detected from space. These have usefully shown regions in which wildfires are common; provided a means of detecting and localizing fires; and for very large fires, identified general fire shape and reaches of active burning (Menzel & Prins, 1996; Morisette et al., 2005; Setzer & Malingreau, 1996). Quantitative measures of fire properties from these sensors may be more limited because of sensor saturation, the low resolution of the sensor, or uncertainty about the radiance of the surface outside of the fire front that contributes to a measurement. Low resolution furthermore limits understanding of fire behavior that is readily apparent in high-resolution airborne measurements (Fig. 6.7).

Riggan et al. (2000) considered the effect of observation scale by simulating the radiant properties of a reach of complex fire line, in the Brazilian Cerrado, as measured with an airborne extended-dynamic-range imaging spectrometer. The simulation considered the fire as viewed in isolation with differing amounts of background at temperatures typical of unburned Cerrado vegetation (at 30°C) or black ash warmed by solar heating (at 70°C). The question asked was: what scale of measurement is required to estimate a useful fire property such as the total fire radiant-flux density? The answer depends on the wavelengths chosen for observation.

The hot-pixel data from within a 50- by 50-m reach of the Serra do Maranhão fire (Riggan et al., 2004) were considered first in isolation: the

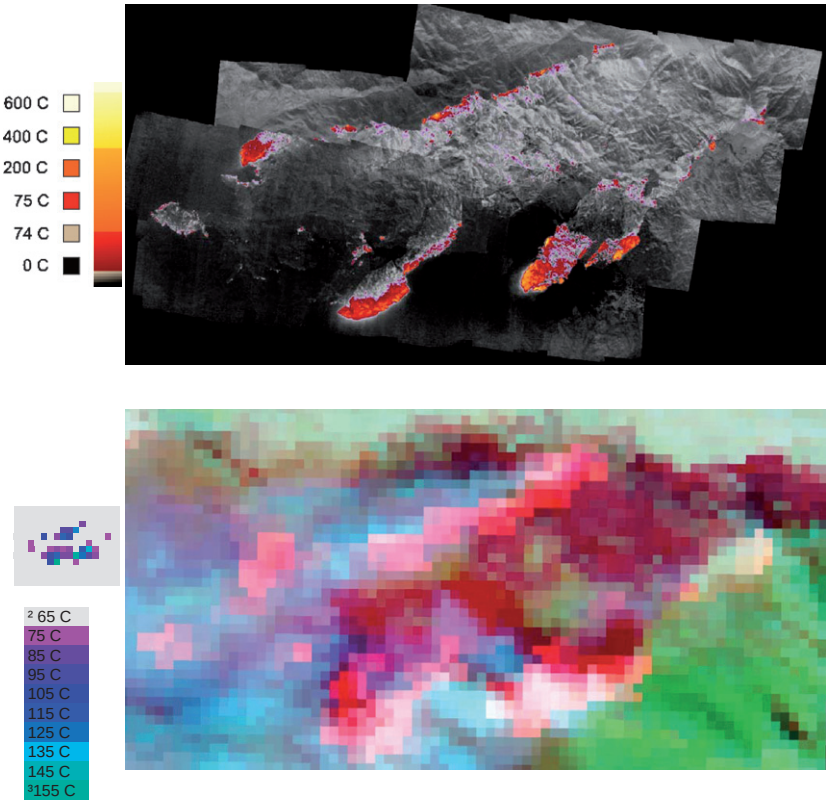

Figure 6.7. Esperanza Fire, Riverside County, CA, October 26, 2006. Color-coded surface temperatures (in Celsius), which reflect fire intensity, are presented as imaged at 14:12 Pacific Standard Time (PST) by the FireMapper at 11.9-μm wavelength in the thermal infrared (top) and compared with radiances at wavelengths of 2.1 μm (mapped in red), 0.85 μm (in green), and 0.65 μm (in blue) as measured at 14:05 PST by the NASA Moderate Resolution Imaging Spectrometer, MODIS (bottom). The MODIS 2.1-μm channel has a nominal resolution of 500 m. The MODIS band-21 fire channel at 3.96 μm, with nominal resolution of 1 km, is shown as a color-coded brightness temperature (inset at left). Here, a moderate Santa Ana wind is driving the fire to the southwest through light fuels and chaparral. By comparison to high-resolution FireMapper data, the MODIS provides approximate fire location and only a general sense of fire activity with little quantitative information regarding fire properties.

radiant-flux density, $3629\,\mathrm{J\,m^{-2}\,s^{-1}}$, estimated with the two-channel method from the summed radiances at wavelengths of 1.63 and 3.9 μm was a close approximation to that obtained by summing the radiant-flux density values from incorporated high-resolution pixels, $3638\,\mathrm{J\,m^{-2}\,s^{-1}}$.

A somewhat less successful estimate of 3537 $J\,m^{-2}\,s^{-1}$ resulted from use of the summed radiances at 3.9 and 11.9 μm. Thus, considering fire-associated areas alone, a coarse-resolution measurement of radiances might produce a reasonable estimate of radiant-energy release given the diversity of incorporated temperatures and values of emissivity-fractional area.

As increasing amounts of relatively low-temperature background of either unburned vegetation or ash were included in the observation, the radiance was quickly elevated at wavelengths longer than 6 μm, but radiances at shorter wavelengths were little affected. Thus, use of radiances at 1.63 and 3.9 μm to estimate temperature, emissivity-fractional area, and radiant-flux density produced good estimates for pixels with a dimension less than approximately 100 m (Riggan et al., 2000). Daytime observations at scales greater than that dimension could incorporate substantial amounts of reflected solar radiation at 1.63 μm and require a correction for the background radiance. Composition of the background is not critical at scales less than 100 m; uncertainty therein produced only an additional 2% error in the estimated radiant-flux density.

Estimates of high-temperature properties from radiance of a low-resolution pixel using two wavelengths including the long-wave infrared will largely fail without some correction for the background. For a 75-m pixel, use of the 3.9 and 11.9 μm wavelengths produced an estimated bulk temperature, 435°C, that described neither the hot elements at 834°C nor the background at 30°C (Riggan et al., 2000). A background correction to the long-wave radiance is problematic since fires generate an ash layer that under solar heating may be at least 72°C (Riggan et al., 1994), 40–45°C warmer than unburned vegetation, and there is no way to know a priori the proportion of these differing targets within a low-resolution pixel. Since the background may be all ash or all unburned vegetation, and the magnitude of this uncertainty amounts to half of the simulated fire signal in a 125-m pixel and over twice the fire signal at 250-m resolution, this approach must fail when pixel sizes greater than about 50 m are used to view the fire. At that scale the uncertainty is only 3% of the fire signal.

6.2.4. High-resolution fire measurement with long-wave-infrared remote sensing

Whereas flame radiance provides an observation of the immediate character of a fire front, measurements at long-wave infrared wavelengths provide a longer-lived, integrating signal of heat absorbed and reradiated by the ground surface over the period from fire-front passage to the time

of observation. This is readily apparent in successive FireMapper observations at 11.9 μm wavelength over the 2005 Woodhouse Fire in Riverside County, CA (Fig. 6.8). The Woodhouse Fire burned in the afternoon and evening of October 25, 2005, under moderate offshore winds, in a Mediterranean-type ecosystem with plant communities composed of chaparral and coastal sage scrub. Over the period of successive fire-line observations from 17:10 to 19:15 Pacific Daylight Time, the head of the fire spread with the wind to the west-southwest at a rate of $0.25\,m\,s^{-1}$; the northern flank of the fire spread lateral to the ambient wind at $0.14\,m\,s^{-1}$. Wind speed at nearby Beaumont, CA, 16 km east of the fire, averaged $5\,m\,s^{-1}$ with gusts to $14\,m\,s^{-1}$. Observed radiometric temperatures at and behind the fire front were affected by both the time since fire passage and the local fire intensity, which apparently reflected local fuel consumption. Based on the rate of spread, temperatures for 1–1.5 h remained elevated above those of black ash, which attained 60°C when heated only by insolation. Thermal data alone qualitatively reproduced the landscape vegetation patterns visible in prefire color-infrared photography, which depicts heavier fuel loadings in chaparral on north-facing aspects and along stream courses, and relatively low fuel loading in coastal sage and grass on ridgelines and south-facing aspects (Fig. 6.9).

6.3. FireMapper applications

The Forest Service's PSW Research Station is developing synoptic-scale fire and environmental data to understand and model the behavior and effects of large wildland fires, including the effects thereon of landscape-scale fuel patterns and treatment. The project supports a Forest Service initiative in which advances in our fundamental understanding of the behavior and immediate impacts of wildland fires are required to provide a firmer basis for fire and fuel management and to enhance public safety, ecosystem sustainability, and environmental quality. While conducting fundamental fire research, we are also developing means for rapid communication, dissemination, and application of the fire intelligence data, and applications of fire imaging in airborne fire operations.

The FireMapper thermal-imaging radiometer has been deployed aboard the PSW Airborne Sciences Aircraft, N70Z, a twin-engine Piper Navajo, since 2000. PSW acquired fire intelligence and provided data to the California interagency Southern Operations Coordination Center during the October 2003 fire emergency in southern California. Data from the FireMapper documented during critical periods the progress

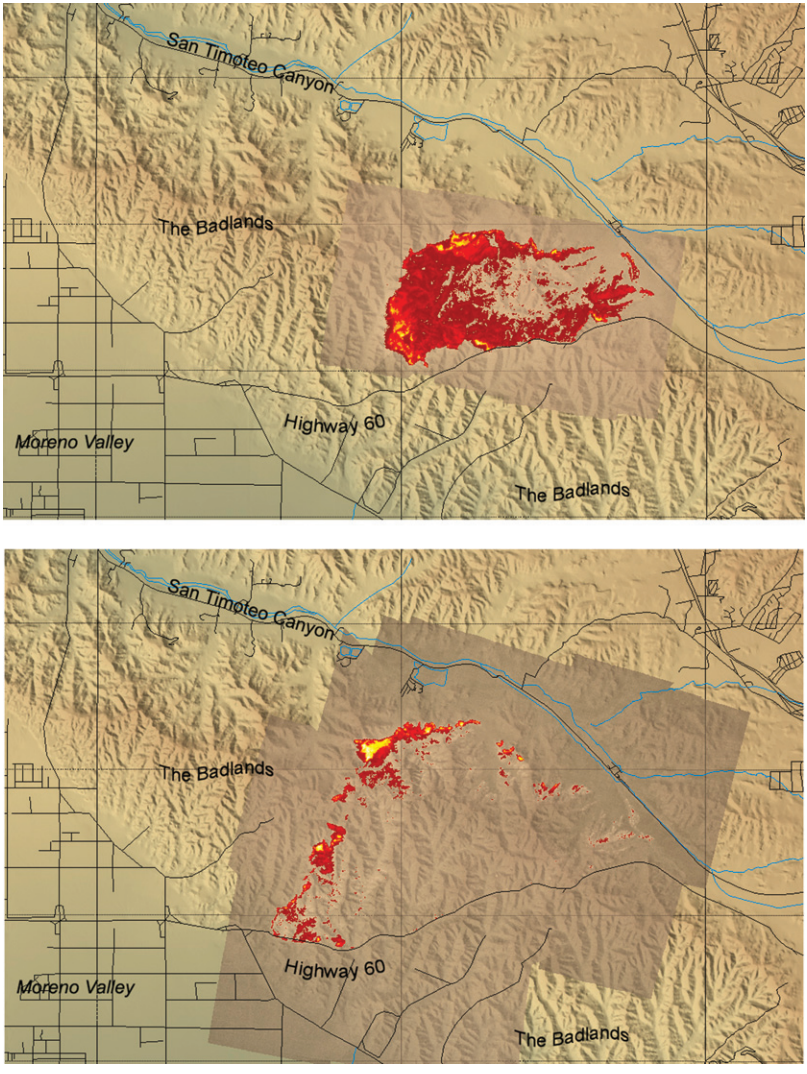

Figure 6.8. Ground temperatures behind the front of the October 5, 2005, Woodhouse Fire, Riverside County, CA, as estimated from radiances measured, at a wavelength of 11.9 μm, with the FireMapper thermal-imaging radiometer. The fire progression is shown from overflights at approximately 17:11 (top) and 19:15 Pacific Daylight Time (bottom). Such color-coded fire information is readily interpretable as to fire location, direction and rate of spread, and activity. Data are shown on shaded topographic relief as posted in near-real time to the Internet at http://www.fireimaging.com/.

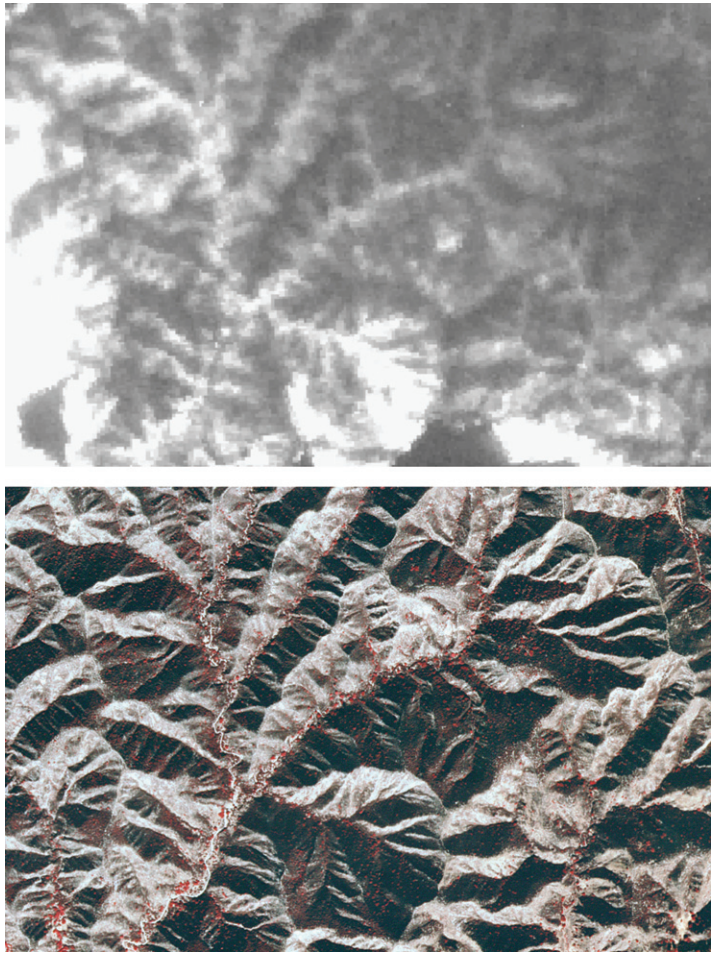

Figure 6.9. Ground-surface temperatures (top) behind the front of the October 5, 2005, Woodhouse Fire, Riverside County, CA, as estimated from radiances measured at 11.9 μm with the FireMapper thermal-imaging radiometer, shown with prefire color-composite photography (bottom) from a U.S. Geological Survey digital orthorectified quarter quadrangle. Images are oriented with north at the top. Residual heat from passage of the fire front, which is located to the west and south of the image, reflects local fuel loading and time since local ignition. Thermal patterns at the top appear to be dominated by fuel loading: bright, high-temperature areas correspond primarily to more north-facing aspects and riparian areas, both of which have relatively contiguous chaparral and woodland and higher fuel loading; dark, cool areas correspond to south-facing aspects with light vegetation, which is primarily annual grasses and coastal sage scrub.

and intensity of the 112,000-ha Cedar Fire and the Old, Grand Prix, Cedar, and Paradise fires, which collectively destroyed thousands of homes in San Bernardino and San Diego counties (Figs. 6.10a and 6.10b). Imagery from the Old and Cedar fires documented fire behavior in chaparral and forest fuels including effects of extensive forest mortality caused by drought and bark beetles. In conjunction with the Forest Service's Missoula Fire Sciences Laboratory, the PSW FireMapper system was deployed for wildfire measurements and intelligence gathering for the Multi-Agency Coordination Group in Missoula, Montana, during the Montana fire emergency in August 2003. Image mosaics depicting

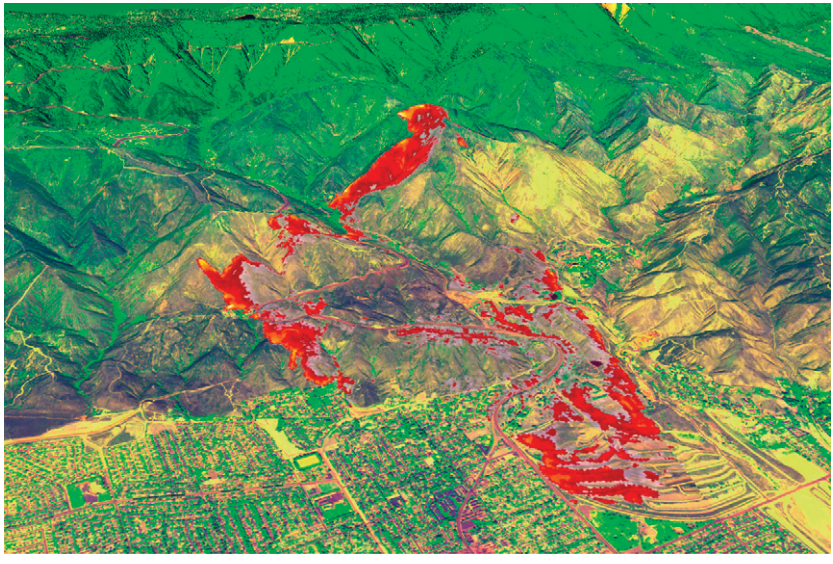

Figure 6.10a. Old Fire, San Bernardino County, CA, as viewed from the southwest at 11:14 Pacific Daylight Time, October 25, 2003, by the PSW FireMapper thermal-imaging radiometer. Color-coded surface temperatures, which reflect fire intensity, are presented as measured in the thermal infrared and posted as an off-nadir overlay on a prefire, multispectral image (with red, near-infrared, and thermal-infrared light shown in red, green, and blue) at http://www.fireimaging.com. Here, a moderate Santa Ana wind is driving the fire to the south and southeast through chaparral and light fuels on hillsides into urban vegetation and structures in the City of San Bernardino. Note the lack of fire activity where the Old Fire encountered the perimeter of the June 1–7, 2002, Arrowhead Fire (yellow vegetation at right of center). Fire at the lower right is burning on a spreading ground, which is used to recharge groundwater. At the time of this image there was little fire activity in the urban area below the burned foothills at lower center.

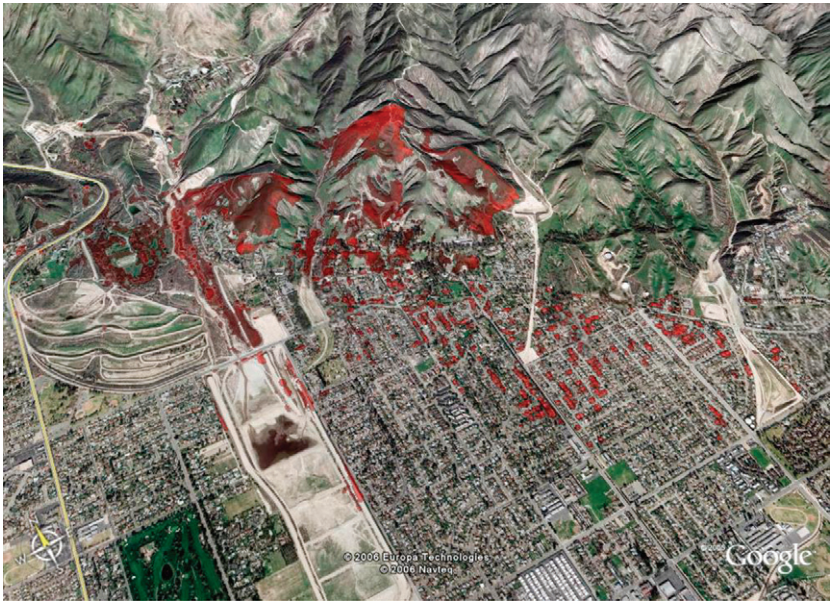

Figure 6.10b. Old Fire, Del Rosa neighborhood, City of San Bernardino, as viewed from the southwest at 13:56 PDT, October 25, 2003, by the PSW FireMapper. Color-coded surface temperatures are presented as an off-nadir overlay in Google Earth as shown as a standard product in near real time at http://www.fireimaging.com/. Here the fire has progressed into the urban area partly by wind-blown fire brands, a large portion of which apparently originated from eucalypts, palms, or other urban vegetation. A long fire incursion is visible along a flood-control facility at lower left-center. Fire-involved structures are readily identified in this image; rapid communication of such imagery could aid firefighters in showing the extent of the fire's incursion into the city and the location of newly involved structures.

fire activity of both small and large-scale incidents were created and disseminated via the Internet for use in strategic planning and operations by incident command teams. FireMapper data were incorporated into a geographic information system (GIS) database by a quick-response team from the Missoula Fire Laboratory and the University of Montana, and data were used to initialize and calibrate FARSITE simulations of behavior of active fires.

FireMapper data are typically acquired from a series of parallel, overlapping passes over a wildland fire. An absolute, through-the-lens calibration with a blackbody of known temperature is performed prior

to each pass. Images are examined in flight and fire data are extracted, compressed with JPEG 2000 wavelet-compression software, and transmitted by File Transfer Protocol (FTP) to a dedicated FTP server via a Qualcomm, Inc., Medium Data Rate Satellite Communications System using the Globalstar network. Aircraft location and attitude data are provided at 20 Hz by a Northrop-Grumman LN-100GT inertial navigation system; these data are associated with imagery in postcollection processing aboard the aircraft. After transmission, fire imagery is decompressed and extracted by a ground-based analyst and orthorectified and associated into large-area mosaics using a Leica Fire Rectification Engine running the Leica Photogrammetry Suite Core software. The rectified thermal imagery is color coded by temperature and posted to the Internet at http://www.fireimaging.com. Products include fire visualizations on shaded relief in a Zoomify viewer based on Adobe Flash technology, in Google Earth, in Google Maps, and as downloadable Geo-TIFF imagery or shape files. The Zoomify viewer allows one to extract the precise location of spot fires or quickly map a fire perimeter over the Internet. Processed imagery from small fires has been posted to the Internet with a best delivery time of 10 min. This rate is sufficient to allow an incident command to use the data to take informed tactical actions, such as backfiring, that could affect the course of a fast-moving fire front. Imagery from large fires, such as the 16,000-ha Esperanza Fire in southern California (Fig. 6.7), has been processed and posted to the Internet within 45 min.

The FireMapper 2.0, a compact second-generation fire remote-imaging radiometer, has been developed by PSW and Space Instruments, Inc., as a commercially available product for routine use in fire research and management. The FireMapper 2.0 incorporates an uncooled BAE Systems, Inc., microbolometer focal-plane array; provides a broad-band thermal-infrared channel encompassing wavelengths from 8 to 12.5 μm and narrow-band channels at 8.8–9.1 μm and 11.3–12.4 μm that each provide unsaturated data over large wildland fires; and implements two levels of quantitative onboard thermal calibration that correct anomalies in image pattern and drift. A FireMapper 2.0 was first deployed in fire operations during the 2004 fire season aboard a firefighting aircraft employed as an aerial supervision module by the USDI Bureau of Land Management. The instrument's small size and weight, compared with the prototype FireMapper, allows it to be operated in a forward-looking, tactical mode to provide images of fire locations and retardant drops during lead-plane operations as well as in a nadir-looking, strategic mode for fire area and intensity mapping. Fire mapping data have been collected in the southwest United States and in Alaska.

6.4. Future missions

PSW is targeting FireMapper to address elements of the Forest Service strategic plan for fire research including (1) transitions and thresholds in fire behavior, (2) fire behavior in complex fuels including live vegetation, (3) physical interactions of fire with the atmosphere, (4) effects of fuel distribution and treatment on subsequent fire behavior, (5) landscape-scale fire processes, and (6) the role of wildland fire in global climate change.

6.4.1. Fire behavior transitions and thresholds

Potentially dangerous and unpredicted transitions in fire behavior, such as from ground-surface fire to crown fire, can compromise firefighter and public safety, tactical fire control, and the protection of communities and natural resources. Small and seemingly "well-behaved" fires may respond to changes in atmospheric conditions or encountered fuel loading and structure, and with little or no warning, become fast moving and highly energetic with catastrophic consequences. Operational fire behavior models are not now capable of successfully predicting these critical transitions in behavior. Transitions to extreme flammability—and potentially severe fire behavior and effects—could also result from prolonged drought stress in forests, woodlands, and chaparral. Qualitative changes in forest flammability are now a critical problem across several regions in the western United States, and especially in southern California, where the fire potential involves interactions of climate variability, forest stand density and structure, pathogens, air pollution, and population growth that place resources and communities at greater risk. Investigation of explosive fire growth requires synoptic fire measurements to document the rates of growth and effects of fuel condition in dynamic and altered ecosystems.

6.4.2. Fire in complex fuels

Fire and fuel management decisions are currently based in part on predictions from semi-empirical and computationally simple models of quasi-steady-state fire spread (Albini, 1976; Finney, 1998; Rothermel, 1972) that have been derived largely from observations of combustion in a laboratory with narrow, homogeneous fuel arrays and flame lengths on the order of 1 m. These models cannot be applied with confidence to simulate burning with high rates of energy release and conditions producing flames tens of meters in length in typically complex terrain and

heavy forest or chaparral fuel, which are vertically stratified, spatially heterogeneous, and comprise a mixture of live and dead biomass. Observations of fire behavior under field conditions are required to validate or invalidate existing models and develop statistical models that describe fire behavior in macroscopic assemblages of fuels.

6.4.3. Interactions of fire with the atmosphere

Fire behavior at scales from a meter to several kilometers may be strongly influenced by the interaction of fire with atmospheric motions, specifically fire-generated winds and winds in complex terrain. At scales of one to tens of meters, fire spread is subject to wake effects (Rodman Linn, personal communication) and is a non-linear function of the length of the combustion zone perpendicular to the direction of spread (Fendell et al., 1990; Jean-Luc Dupuy, personal communication), possibly due to development of horizontal vortices above that zone. At larger scales, fire-modified winds and larger circulations in the atmospheric boundary layer, such as the waves that develop downstream of mountains, may locally accelerate or deform the fire front (Janice Coen, personal communication). Very long fire lines will develop multiple plumes and fire runs. Vorticity on the edges of large plumes can unexpectedly develop destructive fire whorls with strengths approaching those of tornados. Firefighters reportedly faced such extreme fire behavior during the 2003 fire emergency in southern California. Operational fire models do not account for such interactions of fire and the atmosphere, although there are general guidelines for anticipating dangerous fire behavior. More complex research models, such as the Firetec model developed at Los Alamos National Laboratory (Linn, 1997), numerically solve equations describing transport of mass, momentum, and energy in a fire environment. These explicitly describe interactions of fire with the atmosphere—including fire-generated winds—and provide a means to simulate fire behavior in nonhomogeneous fuels and terrain and rapidly changing weather. Direct and synoptic observation of wildland fires is needed to ascertain the importance of macroscale effects in fire behavior—above those of local conditions—such as the effects of long-range spotting in different fuel types or the influence of a fire plume on fire-line shape and to parameterize and validate the new class of fire–atmosphere models.

6.4.4. Fuel treatment influences on fire behavior

Land managers are often tasked to design and implement fuel treatments to mitigate or alter the consequences of wildland fire, yet evidence to

document the effectiveness of treatments has been infrequent and largely anecdotal. We have been unable to objectively characterize changes in subsequent fire environments caused by such management practices as forest thinning, pruning, or harvesting or by prescribed burning in chaparral. Treatments should be designed with consideration of microclimate, fuel structure, and heterogeneity on the landscape, and the subsequent development of fuels, but such effects are not well known. Synoptic-scale, remote measurements of active fires give a means to test the ultimate efficacy of fuel treatments, but the remote sensing will have to largely provide a characterization of the fuels as well.

6.4.5. Landscape and large-scale fire processes

Landscape-scale mapping, assessment, and simulation of wildland fires is needed in order to predict and monitor the cumulative and interactive influences on wildland fire regimes of weather and climate, terrain, ecosystem and fuel development, and fire management. Current strategic planning is largely derived from simulation of fire behavior in static fuels conceptually removed from the landscape, vegetation patch dynamics, climate extremes, persistent fuel boundaries, or dynamic system considerations. This severely limits our ability to predict the resource or societal outcomes of different levels of intervention by fuel or fire management and thereby to defend such a program to the public or regulatory agencies. Large-scale direct impacts of fires are also important in issues of ecosystem response to environmental change, ecosystem restoration to a fire-resilient state, and management of regional air quality and carbon sequestration. Our present knowledge of large-scale dynamics is limited to such measures as decadal trends in cumulative burned area and historical or anecdotal observations of vegetation change. An improved understanding of these processes will require large-scale fire measurements of a large number of fires over time.

6.4.6. Wildland fires in global climate change

Wildland fires may now be contributing to climate change depending on their extent and the strength of their emissions. Best available estimates have considerable uncertainty but do show that biomass combustion is likely a globally important source of atmospheric aerosols, methane, hydrocarbons, carbon monoxide, carbon dioxide, methyl bromide, and nitrous oxide (Crutzen & Andreae, 1990; Radke et al., 1991).

Fires may contribute to global warming to the extent that they reduce the amount of carbon accumulated in standing biomass or soils, as occurs during burning of slashed forest for shifting agriculture or permanent conversion to pasture in the tropics or accelerated burning rates in Mediterranean or temperate climates. A substantial net carbon loss may also occur during dry-season burning of wetlands or due to progressive fire-associated loss of plant nutrients and productivity in ecosystems subject to frequent fires. Fires may also contribute to warming to the degree that they emit higher proportions of methane than would alternative pathways of organic matter decomposition since methane absorbs radiation more strongly than does carbon dioxide. Furthermore, combustion is a copious source of carbon monoxide; microbial decomposition is not. Carbon monoxide (CO) affects the atmospheric concentration of hydroxyl radical (Crutzen & Andreae, 1990), and thereby the residence time of methane and other radiatively important tropospheric species. Thus, increased carbon mineralization by fire yields CO emissions that also contribute to global warming.

High-resolution, remote measurement of wildland fires will be important in ascertaining the importance of global burning in climate change. Existing satellite-based remote sensing can track areas burned over large regions, but high-resolution monitoring will be required to estimate rates of carbon flux to the atmosphere and the degree of residual combustion that is related to emissions of carbon monoxide and other radiatively important trace gases.

6.5. Conclusions

A timely and synoptic view of wildland fire behavior is needed in fire management to efficiently allocate resources during fire-suppression operations; protect firefighters, the public, and our communities; reduce losses of natural resources; and develop our ability to predict the outcome of catastrophic fires. Modern airborne remote-sensing can provide needed quantitative mapping of fire properties including fire-front location, spread, and acceleration; flame temperature, emissivity, and areas; long-distance spotting; radiant-energy emissions; soil heating; residual combustion; and by inference, sensible heat and carbon fluxes to the atmosphere. Low-resolution fire observations at kilometer scale by satellite-based remote sensors readily detect fire radiant emissions and have been usefully applied to detect and localize fires, identify general fire shape and regions of active burning, and map the areas of large fires from changes in surface reflectance. High-resolution measurements at a scale of

one to a few meters, as provided by specialized airborne sensors designed to accommodate the high radiance of wildland fires, are required to quantitatively measure thermal properties associated with active combustion.

Useful fire measurements can be made in high-transmittance atmospheric windows at wavelengths longer than 1.6 μm. Peak radiance from flames occurs at a wavelength of approximately 2.2 μm. Observations of wildland fires in Brazilian Cerrado or savanna vegetation suggest that hot ground and ash within flaming fronts contributes approximately 4% of the radiance at 1.63 μm, three-fifths of the radiance at 3.9 μm, and nearly nine-tenths of the radiance at 11.9 μm. Relative contributions of flames and hot ash to observed fire radiances can be resolved by an iterative method employing the solution of two Planck functions describing radiances at 1.6 and 3.9 μm (the two-channel method) with corrections derived from the long-wave or thermal infrared radiance at 11.9 μm. Single-channel radiance measurements using a wavelength of 11.9 μm have been usefully applied to map approximate ground-surface temperatures associated with burning; a highly resolved time course of this measurement provides a measure of soil heating and fire radiant-energy flux. Measurements of fire radiance at 1.6 and 3.9 μm alone have provided provisional but promising measures of whole-fire sensible energy flux and carbon flux to the atmosphere. Fire radiance at 3.9 μm alone was shown to provide a good estimator of the radiant-flux density estimated from the two-channel method.

PSW is applying synoptic measurements and mapping with its FireMapper thermal-imaging radiometer to characterize the behavior of wildland fires in California and the western United States. FireMapper data have provided the first quantitative and readily interpretable fire intelligence in near real time to interagency incident command teams and the public on major fires in the United States.

Measurements with the FireMapper are being applied to provide substantial new knowledge of wildland fire behavior, especially regarding fire behavior transitions and thresholds, fire in complex fuels, interactions of fire with the atmosphere, fuel treatment influences on fire behavior, landscape and large-scale fire processes, and the role of wildland fire in global climate change.

ACKNOWLEDGMENTS

Research reported herein has been supported by the U.S. National Fire Plan; the Joint Fire Sciences Program; the USDA Forest Service, Pacific

Southwest Research Station and International Programs; the U.S. Agency for International Development, Global Change Program; and the Instituto Brasileiro do Meio Ambiente e dos Recursos Naturais Renováveis. We acknowledge contributions to the research by NASA Ames Research Center, Space Instruments, Inc., and Qualcomm, Inc., and we appreciate reviews by James A. Brass, Nancy E. Grulke, and David Weise.

REFERENCES

Albini, F.A. 1976. Computer-based models of wildland fire behavior: A users' manual. U.S. Department of Agriculture, Forest Service, Intermountain Forest and Range Experiment Station, 68 pp.

Crutzen, P.J., and Andreae, M.O. 1990. Biomass burning in the tropics: Impact on atmospheric chemistry and biogeochemical cycles. Science 250, 1669–1678.

Fendell, F.E., Carrier, G.F., and Wolff, M.F. 1990. Wind-aided firespread across arrays of discrete fuel elements. Defense Nuclear Agency, Technical Report DNA-TR-89-193, Alexandria, VA, 131 pp.

Finney, M.A. 1998. FARSITE: Fire Area Simulator-Model development and evaluation. U.S. Department of Agriculture, Forest Service, Rocky Mountain Research Station, Research Paper RMRS-RP-4, 47 pp.

Linn, R.R. 1997. A transport model for prediction of wildfire behavior. Ph.D. Dissertation, New Mexico State University; also published as Los Alamos National Laboratory Report LA-13334-T.

Liou, K. 1980. An introduction to atmospheric radiation. Academic Press, International Geophysics Series, Vol. 26, London, England, p. 392.

Matson, M., and Dozier, J. 1981. Identification of subresolution high temperature sources using a thermal IR sensor. Photogrammetric Eng. Remote Sens. 47, 1311–1318.

Menzel, W.P., and Prins, E.M. 1996. Monitoring biomass burning with the new generation of geostationary satellites. In: Levine, J.S., ed. Biomass burning and global change, Vol. 2: Biomass burning in the tropical and temperate ecosystems. The MIT Press, Cambridge, MA, pp. 56–64.

Miranda, H.S., Rocha e Silva, E.P., and Miranda, A.C. 1996. Comportamento do fogo em queimadas de campo sujo. In: Anais do Simpósio Impacto das Queimadas sobre os Ecossistemas e Mudanças Globais. 3^0 Congresso de Ecologia do Brasil, 6 a 11 de outubro de 1996, Brasília-DF, 1–10.

Morisette, J.T., Giglio, L., Csiszar, I., and Justice, C.O. 2005. Validation of the MODIS active fire product over Southern Africa with ASTER data. Int. J. Remote Sens. 26, 4239–4264.

Ottmar, R.D., Vihnanek, R.E., Miranda, H.S., Sata, M.N., and Andrade, S.M. 2001. Stereo photo series for quantifying Cerrado fuels in central Brazil–volume 1. U.S. Department of Agriculture, Forest Service, Pacific Northwest Research Station, Portland, Oregon, USA.

Radke, L.F., Hegg, D.A., Lyons, J.H., Hobbs, P.V., Laursen, K.K., Weiss, R.E., Riggan, P.J., and Ward, D.E. 1991. Particulate and trace gas emissions from large biomass fires in North America. In: Levine, J.S., ed. Global biomass burning: Atmospheric, climate, and biospheric implications. The MIT Press, Cambridge, MA, pp. 209–224.

Riggan, P.J., Brass, J.A., and Lockwood, R.N. 1993. Assessing fire emissions from tropical savanna and forests of central Brazil. Photogrammetric Eng. Remote Sens. 59(6), 1009–1015.

Riggan, P.J., Franklin, S.E., Brass, J.A., and Brooks, F.E. 1994. Perspectives on fire management in Mediterranean ecosystems of southern California. In: Moreno, J., and Oechel, W., eds. Fire and Global Change in Mediterranean Ecosystems. Ecological Studies no. 107, Springer-Verlag, New York, 140–162.

Riggan, P.J., Weirich, F.H., DeBano, L.F., Jacks, P.M., Lockwood, R.N., Colver, C., and Brass, J.A. 1994. Effects of fire severity on nitrate mobilization in watersheds subject to chronic atmospheric deposition. Environ. Sci. Technol. 28(3), 369–375.

Riggan, P.J., Hoffman, J.W., and Brass, J.A. 2000. Estimating fire properties by remote sensing. Proceedings of the IEEE Aerospace Conference, Aspen, Colorado, Paper no. 519.

Riggan, P.J., and Hoffman, J.W. 2003. FireMapper™: A thermal-imaging radiometer for wildfire research and operations. Proceedings of the IEEE Aerospace Conference, Big Sky, Montana, Paper no. 1522.

Riggan, P.J., Tissell, R.G., and Hoffman, J.W. 2003. Application of the FireMapper™ thermal-imaging radiometer for fire suppression. Proceedings of the IEEE Aerospace Conference, Big Sky, Montana, Paper no. 1523.

Riggan, P.J., Lockwood, R.N., Tissell, R.G., Brass, J.A., Pereira, J.A.R., Miranda, H.S., Miranda, A.C., Campos, T., and Higgins, R. 2004. Remote measurement of wildfire energy and carbon flux from wildfires in Brazil. Ecol. Appl. 14(3), 855–872.

Rothermel, R.C. 1972. A mathematical model for predicting fire spread in wildland fuels: U.S. Department of Agriculture, Forest Service, Intermountain Forest and Range Experiment Station, 40 pp.

Setzer, A.W., and Malingreau, J.P. 1996. AVHRR monitoring of vegetation fires in the tropics: Toward the development of a global product. In: Levine, J.S., ed. Biomass burning and global change, Vol. 2: Biomass burning in the tropical and temperate ecosystems. The MIT Press, Cambridge, MA, pp. 25–39.